Effect of the Hadley Circulation on the Reflection of Planetary Waves in Three-Dimensional Tropospheric Flows

CHRISTOPHER C. WALKER AND GUDRUN MAGNUSDOTTIR

Department of Earth System Science, University of California, Irvine, Irvine, California

(Manuscript received 3 December 2001, in final form 4 April 2002)

ABSTRACT

The nonlinear behavior of quasi-stationary planetary waves excited by midlatitude orographic forcing is considered in a three-dimensional primitive equation model that includes a representation of the Hadley circulation. The Hadley circulation is forced by Newtonian cooling to a zonally symmetric reference temperature and vertical diffusion on the zonally symmetric component of the flow. To quantify the effect of the Hadley circulation on wave propagation, breaking, and nonlinear reflection, an initial state with no meridional flow, but with the same zonal flow as the Hadley state, is also considered. In order to allow the propagation of large-scale waves over extended periods, Rayleigh friction is applied at low levels to delay the onset of baroclinic instability.

As in the absence of a Hadley circulation, the waves in the Hadley state propagate toward low latitudes where the background flow is weak and the waves are therefore likely to break. Potential vorticity fields on isentropic surfaces are used to diagnose wave breaking. Nonlinear pseudomomentum conservation relations are used to quantify the absorption–reflection behavior of the wave breaking region. In the presence of a Hadley circulation representative of winter conditions, the nonlinear reflection requires more forcing to get established, but a reflected wave train is still present in the numerical simulations, both for a longitudinally symmetric forcing and for the more realistic case of an isolated forcing. The effect of the thermal damping on the waves is more severe in the current three-dimensional simulations than in the shallow water case considered in an earlier study. Both the directly forced wave train and the reflected wave train are quite barotropic in character; however, in the shallow water case one is essentially assuming an infinite vertical scale.

1. Introduction

Recent modeling studies have presented evidence that large-amplitude planetary waves propagating from the midlatitudes toward the Tropics are, after an initial period, reflected back toward the midlatitudes (Brunet and Haynes 1996; Magnusdottir and Haynes 1999, hereafter MH99; Magnusdottir and Walker 2000, hereafter MW00; Esler et al. 2000, hereafter EPP). As waves excited in midlatitudes propagate toward the equator, they encounter regions where their zonal phase speed matches the background zonal flow (the critical line) and, if dissipation is small enough, the waves must break. Wave breaking is shown in observational studies by, for example, Hsu et al. (1990), who examined potential vorticity (PV) on isentropic surfaces in the low-latitude upper troposphere, and found the overturning of PV contours associated with breaking waves.

Killworth and McIntyre (1985) proved analytically that the flux of pseudomomentum into the wave breaking region cannot continue indefinitely. They showed that the absorptivity of the wave breaking region is bounded (the KM bound) and will oscillate between absorbing and overreflecting states, asymptoting to a perfectly reflecting state in the long time limit. The KM bound was, however, derived under fairly restrictive assumptions, so its applicability to the atmosphere, or at least to tropospheric flows, was not clear. For the KM bound to hold, the following must be true: (i) the flow is horizontal (two-dimensional) and balanced, (ii) vorticity is not created or destroyed in the wave breaking region (conservative flow), (iii) vorticity is not advected in or out of the region, and (iv) the disturbance is longitudinally periodic.

The modeling studies mentioned above have shown that nonlinear reflection persists even as these assumptions are relaxed. Brunet and Haynes (1996) used a shallow water model and found that reflection can occur in flow that is not balanced and when the wave train is not periodic in longitude. A similar study by Waugh et al. (1994) in a nondivergent barotropic model also noted the reflection of a nonperiodic wave train, although reflection was not the focus of their study. MH99 generalized the results of Brunet and Haynes (1996) to three

Corresponding author address: Dr. Gudrun Magnusdottir, Department of Earth System Science, University of California, Irvine, Irvine, CA 92697-3100.
E-mail: gudrun@uci.edu

dimensions using a primitive equation model. In addition, MH99 departed from the idealized wind profile of Held [1985, which was used by Brunet and Haynes (1996)] and considered flows that are closer to observed wintertime conditions.

Subsequent studies by MW00 and EPP employed a shallow water model to consider wave reflection in the presence of a Hadley circulation. These studies challenged the conditions that there not be any advection of fluid into the wave breaking region, and that vorticity not be created or destroyed in the wave breaking region. Both studies found that the Hadley circulation damps wave reflection, but that given enough forcing, nonlinear reflection can still occur. Through a budget analysis of low-latitude sources and sinks of pseudomomentum, EPP showed that the Hadley circulation damps wave reflection through an indirect mechanism in which the Hadley circulation allows wave breaking to continue indefinitely, thereby increasing the enstrophy cascade to small scales and allowing hyperdiffusion to dissipate more wave activity. MW00 proposed a more direct role for the Hadley circulation: by maintaining the low-latitude PV gradient, the Hadley circulation damps reflection by opposing PV overturning that leads to the nonlinear reflection. In the present study we conduct a similar budget analysis to that of EPP, except for three-dimensional primitive equation flow, and arrive at different conclusions from those of EPP.

Although MW00 and EPP were the first to focus on the effect of the Hadley circulation on nonlinear wave reflection, several studies have investigated other aspects of the interaction between the Hadley circulation and planetary waves. Watterson and Schneider (1987) looked at the effect of the Hadley circulation on linear waves in a three-dimensional model. They found that the opposing meridional flow impeded meridional propagation, effectively displacing the critical line northward. A study by Held and Phillips (1990), using a shallow water model, investigated the interaction of a longitudinally periodic planetary wave with the Hadley circulation. Held and Phillips (1990) did note some evidence for reflection, but this was not the focus of their study.

Here we extend EPP and MW00 by examining nonlinear wave reflection in the presence of a wintertime Hadley circulation in a three-dimensional, primitive equation model. We conduct a series of numerical experiments, varying the shape (longitudinally symmetric or longitudinally asymmetric) and the amplitude of topographical forcing. For each of these different topographies, we run one experiment using an initial state that has a Hadley circulation and a companion experiment with an initial state that does not have a Hadley circulation, but is otherwise the same. Comparing the results from the two sets of experiments isolates the effect of the Hadley circulation on wave propagation, breaking, and reflection.

An outline of this paper is as follows. In section 2 we briefly discuss some preliminaries: the primitive equation model, parameter settings, topography, and our method of forcing a Hadley circulation. Sections 3 and 4 describe the numerical experiments with wave-3 topography and the more realistic case of isolated topography, respectively. In section 5 we discuss our results, especially in comparison with EPP and MW00, and briefly discuss other, complementary experiments not reported on in previous sections. Finally, in section 6, we briefly summarize our results.

2. Some preliminaries

a. Model, parameter settings, and topography

The numerical experiments are performed with the primitive equation model developed by Hoskins and Simmons (1975), run at a horizontal resolution of T42, with 15 sigma levels in the vertical. It is a spectral model that integrates the vorticity, divergence, and temperature equations. Hyperdiffusion (∇^6) is included in the vorticity, divergence, and temperature equations such that the smallest horizontal scales are subject to a 10 per day damping.

Planetary waves are excited in the model through the introduction of topography. The topography has two different shapes: 1) a shape that is Gaussian in both latitude and longitude, located at 40°N, 0°, with a half width of 1066 km (isolated forcing); and 2) a shape that is Gaussian in latitude, centered around 40°N, but that has wave-3 structure in longitude (wave-3 forcing). In both cases, the height of the topography is smoothly increased to its steady-state value over the first 4 days of each simulation. A nondimensional forcing amplitude δ is defined by $\delta = h/h_0$, where h is the maximum height of the mountain and h_0 is 840 m.

As the waves excited by the topography break in low latitudes, it is desirable to have a quantitative measure of the resulting wave breaking region. Similar to Postel and Hitchman (1999), we define the surf zone as the region with a reversed PV gradient. As wave breaking proceeds in time, the wave breaking region grows larger in both latitude and longitude, indicating the ''stage'' of wave breaking. We therefore use the extent of the surf zone to compare wave breaking events from different simulations.

To inhibit the growth of baroclinic instability, linear Rayleigh friction acts on wave components of the flow in the lowest layers of the model. Without Rayleigh friction, baroclinic disturbances grow quickly to obscure the forced planetary response. A drag coefficient of 5 day^{-1} at sigma = 1, decreasing linearly to zero at sigma = 0.7 prevents baroclinic instability for the duration of the 20-day simulations. See MH99 for a discussion of the effect of this low-level Rayleigh friction on wave propagation.

The experimental methods are similar to those in our previous shallow water study (MW00). We consider the

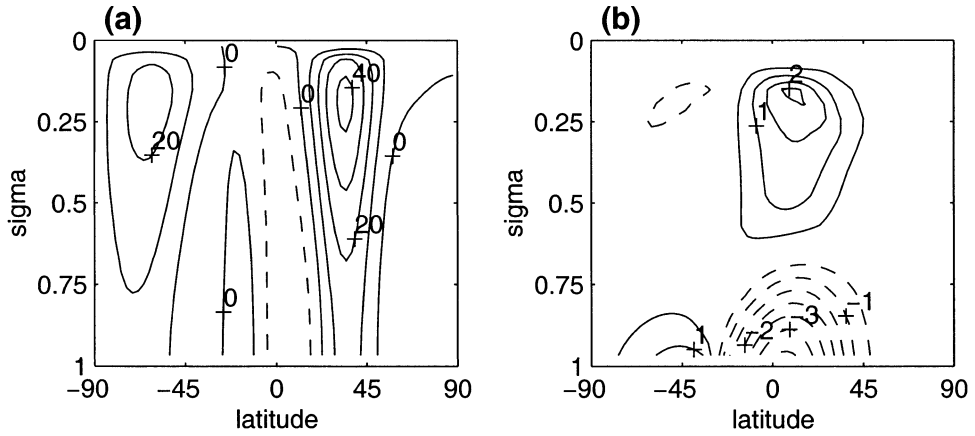

FIG. 1. The axisymmetric initial-state (a) zonal and (b) meridional wind used in numerical experiments including a Hadley circulation. Contour interval is 10 m s^{-1} in (a) and 0.5 m s^{-1} in (b). Dashed contours are negative.

fate of planetary waves on two axisymmetric initial states, a state with a Hadley circulation (the Hadley initial state), and a state with the same zonal wind as the Hadley state, but with no meridional circulation (the no-Hadley initial state). The Hadley state, shown in Figs. 1a and 1b, results when the model is integrated to a steady state while forcing the temperature and momentum (section 2b). This axisymmetric steady state is then used as an initial state for experiments where waves are excited.

To quantify the effect of the Hadley circulation on wave reflection, we compare results from the Hadley initial state with results from the no-Hadley initial state, which has the zonal wind profile shown in Fig. 1a, but does not have any meridional circulation. The temperature and surface pressure fields are determined so that the no-Hadley initial state is in gradient wind balance. The forcings applied to the thermal and momentum equations to generate a Hadley circulation are not present in the no-Hadley experiments.

The presence of the Hadley circulation causes small differences between the PV fields associated with the Hadley and no-Hadley initial states, and we therefore show results on the $\theta = 345$ K surface for the Hadley initial state and on the $\theta = 350$ K surface for the no-Hadley state. These surfaces are chosen because they have a similar gradient of PV in low latitudes. Also, the 345-K surface intersects the low-latitude region of maximum amplitude latitudinal velocity of the Hadley circulation. The 345-K isentropic surface corresponds to approximately $\sigma = 0.18$ in low latitudes. The 350-K isentropic surface of the no-Hadley state corresponds to about $\sigma = 0.15$ in low latitudes.

b. Hadley initial state

We force an axisymmetric Hadley circulation with a combination of 1) a relaxation of the zonally symmetric temperature field toward a specified profile, and 2) vertical diffusion of zonally symmetric momentum. Forcing an axisymmetric Hadley circulation in this manner is familiar from, for example, Held and Hou (1980), and a detailed justification for forcing a Hadley circulation in this way is given there. We discuss here only the details of the forcing that are particular to our study. Note that the role of the thermal relaxation and vertical momentum diffusion is only to produce a Hadley circulation. Both are therefore only applied to the zonally symmetric part of the flow.

1) THERMAL RELAXATION

The model includes thermal forcing of the form

$$\frac{\partial \overline{T}}{\partial t} = \cdots - \frac{\overline{T} - T_r}{\tau}, \tag{2.1}$$

where $\overline{T}$ is the zonally averaged temperature, T_r is a specified zonally symmetric temperature field, and τ is a relaxation timescale, taken here to be 15 days. It is included in the model as a crude representation of dia-

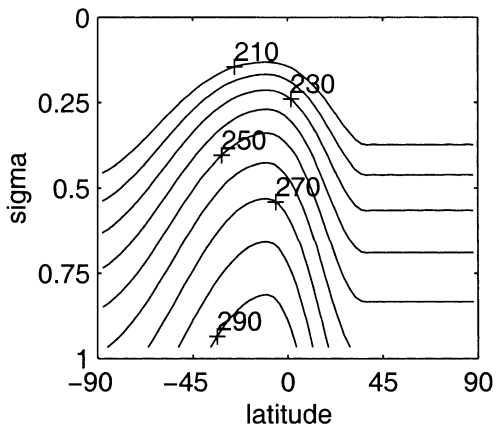

FIG. 2. Thermal relaxation field T_r. Contour interval is 10 K.

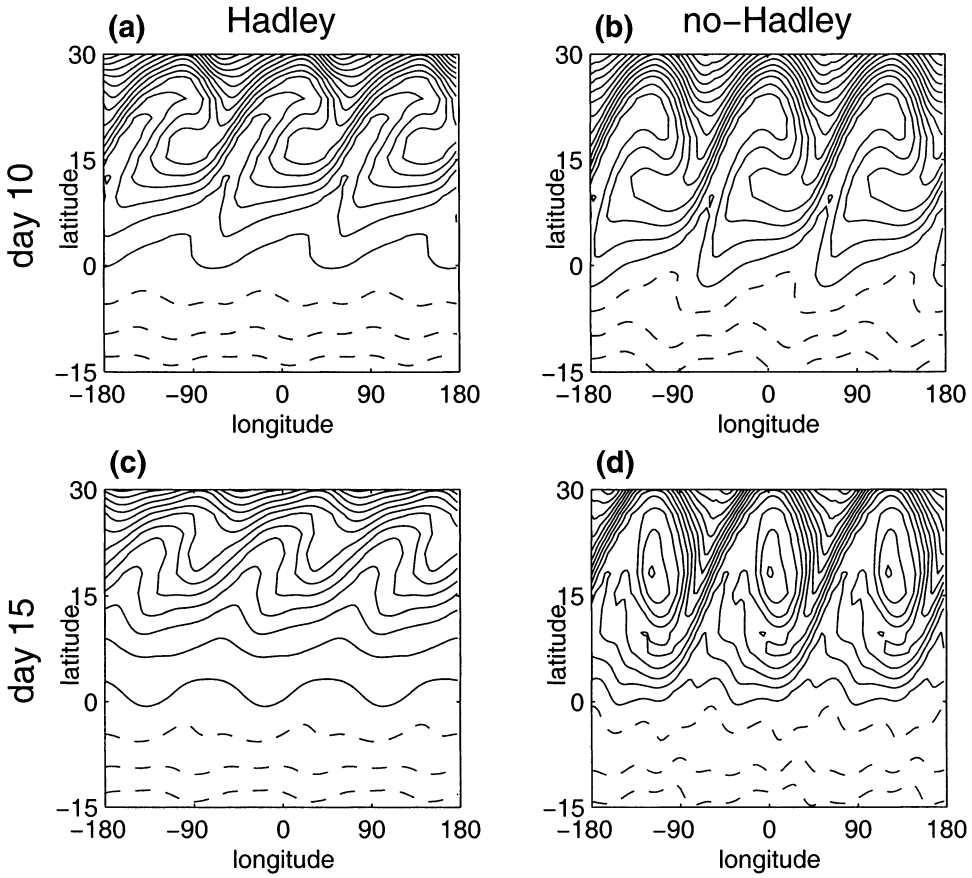

FIG. 3. Potential vorticity for wave-3 forcing with forcing amplitude $\delta = 1.0$ on (a), (b) day 10, and (c), (d) day 15, for the (a), (c) Hadley initial state, and the (b), (d) no-Hadley initial state. Potential vorticity is shown on 345-K surface in Hadley cases and 350-K surface in no-Hadley cases. Contour interval is 0.2 PVU (1 PVU = 10^{-6} m^2 s^{-1} K kg^{-1}) in all cases.

batic effects that are not captured by the model, notably, the release of latent heat at low latitudes associated with convection in the ITCZ, and radiative cooling. The thermal relaxation field (T_r) used in this study is shown in Fig. 2.

2) VERTICAL MOMENTUM DIFFUSION

We include vertical momentum diffusion on the zonally symmetric component of the flow to represent eddy friction. Momentum is diffused in the vertical in the usual way (e.g., Kiehl et al. 1996); that is,

$$\frac{\partial \overline{\mathbf{v}}}{\partial t} = \cdots + \frac{1}{\rho}\frac{\partial}{\partial z}\rho\nu\frac{\partial \overline{\mathbf{v}}}{\partial z}, \tag{2.2}$$

with boundary conditions

$$\frac{\partial \overline{\mathbf{v}}}{\partial z} = 0 \quad \text{at top,} \tag{2.3}$$

$$\nu\frac{\partial \overline{\mathbf{v}}}{\partial z} = C\overline{\mathbf{v}} \quad \text{at bottom.} \tag{2.4}$$

In the above equations, ρ is mass density and $\overline{\mathbf{v}} = (\overline{u}, \overline{v})$ where $\overline{u}$ and $\overline{v}$ are the zonal mean components of velocity in the zonal and meridional directions, respectively. For all experiments investigating wave reflection, $\nu = 75$ m^2 s^{-1} and $C = 0.0001$ m s^{-1}. The presence of vertical diffusion might be expected to have an effect on wave propagation and breaking, especially considering the large value of diffusivity. We examine the effect of vertical diffusion on wave breaking in appendix A.

3. Results for wave-3 forcing

We first discuss wave-3 topography. Several different nondimensional forcing amplitudes (δ) are considered, from forcing amplitude 0.1, which does not show any evidence of low-latitude wave breaking, to forcing amplitude 1.0, which is strongly nonlinear.

Figures 3a–d show PV for $\delta = 1.0$, for the Hadley (left) and no-Hadley (right) initial states, on day 10 (top) and on day 15 (bottom). As discussed in section 2a, PV is shown on the $\theta = 345$ K surface for the Hadley case and on the $\theta = 350$ K surface for the no-Hadley case. The PV fields shown in Figs. 3a–d reveal two main differences between the Hadley case and the no-Hadley

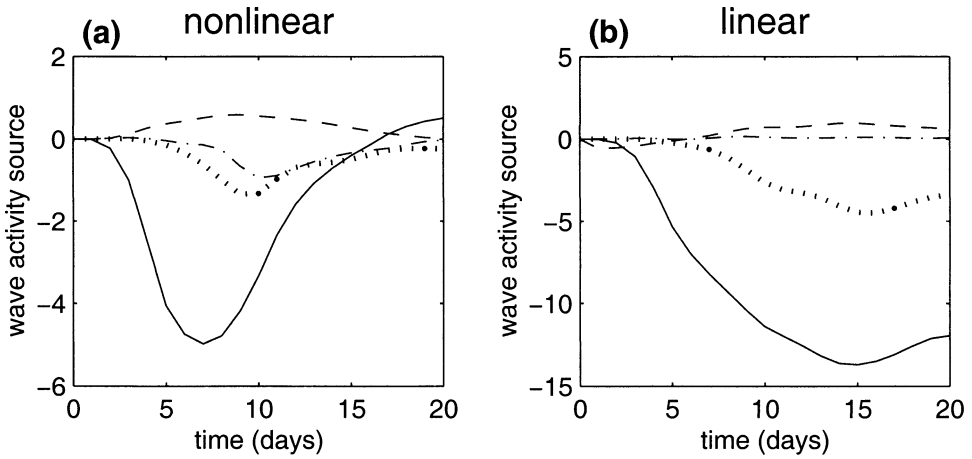

FIG. 4. Time evolution of the volume-integrated terms of S [the pseudomomentum source S from Eq. (B.6)], for wave-3 forcing of (a) amplitude $\delta = 1.0$ and (b) $\delta = 0.1$. Shown are the Hadley dissipation term (solid), eddy heating term (dashed), eddy friction term (dashed–dotted), and hyperdiffusion term (thick dotted). The source terms are dimensionless and scaled by the amplitude of forcing squared. The volume is a zonal strip between the equator and 26.5°N, and between isentropic surfaces of 310 and 380 K.

case. First, they show a northward displacement of wave propagation and breaking, due to the opposing meridional flow in the Hadley circulation. This is in agreement with the earlier shallow water studies (MW00 and EPP) and with Watterson and Schneider (1987), who examined the effect of meridional flow on linear planetary wave propagation in three-dimensional flow and found that the opposing flow displaces the critical line northward.

Second, and more important to wave reflection, the Hadley case shows less PV overturning than the no-Hadley case, after about day 10. Early in the simulation, both cases show similar PV overturning. The PV fields on day 10, for example, show wave breaking with similar surf zone dimensions in both the Hadley and no-Hadley cases. Isolating one of the three wave breaking regions in Figs. 3a and 3b, the surf zone width in longitude is 138° in the Hadley case and 143° in the no-Hadley case. In latitude, the surf zone width is 20° in the Hadley case and 25° in the no-Hadley case.

As the simulation continues past day 10, the no-Hadley PV continues to evolve toward smaller spatial scales, while the Hadley PV stops evolving and even ''unwinds'' slightly as the flow becomes more zonal. This is shown on day 15, in Figs. 3c and 3d. Here, the no-Hadley case (Fig. 3d) is quite disturbed and has isolated patches of PV with small spatial scales, while the Hadley case has a flow that is more zonal than it was on day 10. This trend in the Hadley PV field continues after day 15. On day 20, the PV field in the Hadley case (not shown) is slightly more zonal than the field shown on day 15, despite continuing topographic forcing.

The results shown in Figs. 3a–d are in many respects consistent with earlier results in a one-layer model (e.g., Held and Phillips 1990). The meridional PV gradient is maintained in the presence of a Hadley circulation, whereas without a Hadley circulation, the PV gradient is reduced or, if the forcing is sufficiently strong, completely eliminated. The thermal forcing associated with the Hadley circulation maintains a gradient of PV, even though there is continual wave forcing. Neither EPP nor MW00, however, found that the Hadley circulation caused the flow to become more zonal late in the simulation. We believe that the difference in behavior between the shallow water case and the primitive equations case reveals a difference in the way that thermal relaxation acts in these two models. We are not aware of any studies that compare the effect of thermal forcing on PV fields in two- and three-dimensional models. Haynes and Ward (1993), in a three-dimensional study of the thermal decay of stratospheric PV anomalies, found that the decay rate of a PV anomaly depends on its vertical scale. In particular, they found that deep PV anomalies decay more slowly than shallow PV anomalies. Their results indicate that for a given thermal relaxation damping time τ, the timescale of the response in the shallow water case will be significantly longer than in the baroclinic case studied here.

The evolution of the flow shown in the Hadley state PV field in Figs. 3a and 3c is also apparent in an analysis of S, the nonconservative source/sink of pseudomomentum. Pseudomomentum satisfies the conservation relation (B.1) exactly for finite-amplitude disturbances (see appendix B). Figure 4 shows the time evolution of the volume integrated terms of S [as given in Eq. (B.6)] for wave-3 forcing of two different amplitudes. Figure 4a is for $\delta = 1.0$, which is the case shown in Figs. 3a and 3c. Figure 4b is for a linear forcing amplitude $\delta = 0.1$. (We define ''linear'' amplitudes as those amplitudes where the resulting wave is absorbed indefinitely in low latitudes.) The volume considered is a zonal strip from the equator to 26.5°N and stretching in the vertical from

potential temperature of 310 K, which is slightly above midtroposphere for this latitude band, to 380 K. The curves shown in Fig. 4a reach a maximum amplitude around day 10, when the perturbation from the basic state is at its maximum, and decline thereafter, as the flow reverts to its initial state. This is consistent with the evolution of the PV field, which stops evolving around day 10 and then begins to revert to its original zonally symmetric configuration.

Considering the time period before day 12, the pseudomomentum budget reveals that the Hadley circulation is the primary sink of pseudomomentum, followed by hyperdiffusion and eddy friction, whereas eddy heating is a source of pseudomomentum. This is quite different from the shallow water case shown in EPP (their Fig. 10a), where by day 12 hyperdiffusion is the most important sink of pseudomomentum followed by eddy friction and Hadley cell dissipation. In that case the Hadley cell dissipation remains the same later in the simulation, whereas in the three-dimensional simulation shown in Fig. 4a, the dissipation due to the forcing acting on the basic state drops off quickly after day 7 and changes sign late in the simulation. Figure 4a also shows that the eddy heating term acts as a source of pseudomomentum. This is in contrast to the shallow water case, where eddy heating does not add or remove pseudomomentum from the region.

The time evolution of the various contributions to S for a linear case (forcing amplitude $\delta = 0.1$) is shown in Fig. 4b. Now, the Hadley cell dissipation is the dominant term throughout the simulation, followed by hyperdiffusion. Thus, the Hadley cell dissipation depends sensitively on the amplitude of the disturbance. When the disturbance is strong, thermal forcing pulls the disturbed state to the basic state on rather short timescales, producing the sharp decrease in the Hadley cell dissipation seen in Fig. 4a.

Although the thermal forcing that drives the Hadley circulation tends to resist the PV overturning that is critical to wave reflection, nonlinear reflection is still present in the Hadley case. Figure 5 shows contour plots in the latitude–time plane of the normalized zonally averaged equatorward pseudomomentum flux ($\overline{F^{(\phi)}}$), integrated in the vertical from potential temperature of 310 to 380 K. In all cases, there is a gradual increase in flux associated with the initial growth of the topography, which reaches its steady state after 4 days. For both linear cases ($\delta = 0.1$), the flux reaches a steady state around day 5, slightly earlier for the no-Hadley case. This is indicative of wave trains propagating from midlatitudes to low latitudes, where they are absorbed near their critical level (around 10°N in the upper troposphere). MH99 found similar behavior for small amplitude forcing in nearly inviscid three-dimensional flow.

As the forcing amplitude is increased, the equatorward flux no longer comes to a steady state. Instead, as shown in Figs. 5d and 5f for the no-Hadley case of forcing amplitude 0.7 and 1.0, respectively, the flux increases first, and then abruptly decreases. As MH99 discussed for the nearly inviscid case, this decrease is associated with wave reflection out of the low-latitude wave breaking region. The stronger the forcing the earlier the decrease in flux takes place. We see that an abrupt decrease in flux also takes place in the same amplitude Hadley cases shown in Figs. 5c and 5e. This is indicative of nonlinear reflection.

For both forcing amplitudes, the equatorward flux in the Hadley case is smaller than the equatorward flux in the no-Hadley case. This was not seen in either EPP or MW00. In similar figures, they observed similar values of the of flux in both Hadley and no-Hadley cases. This implies that thermal relaxation has a stronger influence in the primitive equation case than in the shallow water case.

4. Results for isolated forcing

We now turn to isolated topography, which is more relevant for the tropospheric flows considered here. As shown in earlier studies (e.g., Grose and Hoskins 1979), this type of isolated forcing excites two wave trains, one directed eastward and poleward, and the other eastward and equatorward. It is the equatorward-directed wave that is of interest in this study. We consider several values of forcing amplitude δ, from 0.1, which does not display any wave breaking, to 2.0, which shows pronounced wave breaking.

We first consider the nondimensional forcing amplitude of 1.5. Figures 6a and 6c show PV for the Hadley and no-Hadley initial states, respectively, after 10 days of integration. As before, PV is shown on the $\theta = 345$ K surface for the Hadley case and the $\theta = 350$ K surface for the no-Hadley case. Both states show PV overturning around 15°N, 30°W, associated with the breaking of the equatorward-propagating wave train. There are also signs that the poleward-directed wave is breaking in high latitudes, but this is not relevant to this study. The low-latitude wave breaking is at a similar stage in both cases, as determined by the dimensions of the surf zone. (Surf zone dimensions are 8° latitude, 82° longitude in the Hadley case; 11° latitude, 87° longitude in the no-Hadley case.) As in the wave-3 case, the wave breaking region in the Hadley case is displaced northward by the latitudinal flow in the Hadley circulation.

Figures 6b and 6d show pseudomomentum flux (arrows) and density (contours) also for day 10, for the Hadley and no-Hadley cases, respectively. Initially, there is no pseudomomentum at low latitudes. As the simulations progress, both cases show a buildup of pseudomomentum in the wave breaking region. There is approximately twice as much pseudomomentum in the wave breaking region of the no-Hadley case compared to the Hadley case. Figures 6b and 6d also show a flux of pseudomomentum out of the wave breaking region into the subtropics, which we interpret as a signature of

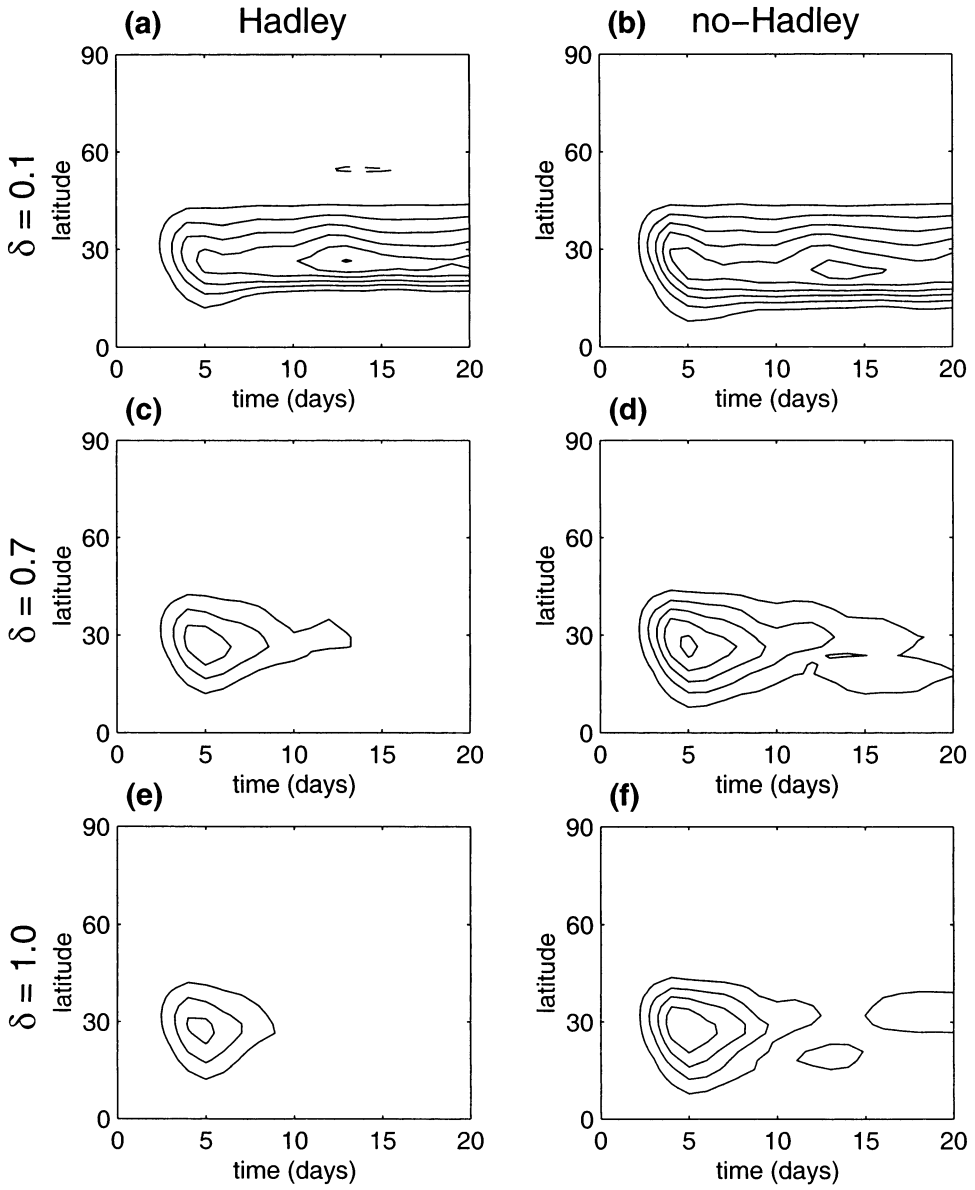

FIG. 5. Time evolution of the normalized, zonal average of southward pseudomomentum flux in the time–latitude plane, integrated vertically from 310 to 380 K, for three different values of δ: (a), (b) linear forcing amplitude 0.1, (c), (d) nonlinear forcing amplitude 0.7, and (e), (f) nonlinear forcing amplitude 1.0. Hadley cases are on the left, no-Hadley cases are on the right.

nonlinear reflection. This flux, which emerges from the wave breaking region around 30°N, 60°W, is substantially larger in the no-Hadley case, in accord with the idea that the Hadley circulation damps wave reflection. Consistent with earlier studies, the flux shows that further downstream the reflected wave arcs back toward the equator where it is dissipated in low latitudes near 15°N, 135°W.

Reflection is also evident for both cases in Fig. 7. Figure 7 is for the same time and the same amplitude forcing as Fig. 6, but it shows the perturbation meridional wind on the $\sigma = 0.2$ surface, for (a) the Hadley state and (b) the no-Hadley state. Both cases show a reflected wave train propagating out of the wave breaking region (around 15°N, 30°W). This reflected wave train propagates toward the midlatitudes, then turns back toward low latitudes, where it is absorbed around 30°N, 150°W. Consistent with Fig. 6, the reflected wave in the Hadley case is weaker than the reflected wave in the no-Hadley state.

As the integration continues past day 10, the isolated cases display the same behavior seen when the waves were forced with wave-3 topography. The no-Hadley flow continues to evolve toward smaller spatial scales

while the Hadley flow becomes more zonal. This is shown in Figs. 8a–d, which are identical to Figs. 6a–d, except on day 15. In the no-Hadley case, Fig. 8b, the PV in the wave breaking region is almost completely homogenized, while the PV in the Hadley case, Fig. 8a, still has a pronounced meridional gradient. As was the case for the wave-3 forcing, the PV field in this isolated forcing Hadley case is more zonal on day 15 than it was on day 10. It is interesting to note that the PV in the Hadley case is at a quasi steady state. On day 20 (not shown), the low-latitude PV field looks almost identical to that shown on day 15. In addition, beginning around day 15, the no-Hadley case displays a secondary wave breaking region around 15°N, 120°W, where the reflected wave impacts the low latitudes. In the Hadley case, the reflected wave is not large enough to generate a secondary wave breaking region. Instead, the reflected wave train is absorbed near the critical line.

The pseudomomentum flux in Figs. 8b and 8d again shows a flux associated with a reflected wave propagating from the wave breaking region into midlatitudes. Although reflection is again visible in both the Hadley and no-Hadley cases, there are two important differences between the pseudomomentum flux fields shown on day 15 (Figs. 8b and 8d) and those shown on day 10 (Figs. 6b and 6d). First, the effect of the Hadley circulation on the amplitude of the reflected wave is much larger on day 15 than on day 10. On day 10, the flux associated with the reflected wave in the Hadley case is approximately one-third the flux in the no-Hadley case. By day 15, the Hadley flux is one-fifth the no-Hadley flux. This is consistent with the evolution of the PV fields, which are similar on day 10, and diverge thereafter. Second, considering the Hadley case, careful examination reveals that the magnitude of the reflected flux is smaller on day 15 than on day 10. This is in accord with the slight unwinding of the PV field between day 10 and day 15. In contrast, the magnitude of the reflected wave in the no-Hadley case is larger on day 15 than on day 10.

The behavior of forcing amplitude 1.5 is compared with other amplitudes in Fig. 9, which shows the time evolution of the zonal average of equatorward pseudomomentum flux ($\overline{F^{(\phi)}}$) through 30°N, integrated from 310 to 380 K. The Hadley case is in Fig. 9a; the no-Hadley case is in Fig. 9b. MH99 showed similar plots for three different no-Hadley states and, based on those plots, argued that nonlinear reflection was occurring. Each flux is normalized by the forcing amplitude squared and multiplied by 1000. Forcing amplitude 0.1 is linear, so that waves are absorbed at low latitudes. This is shown in the amplitude 0.1 profiles as the maintenance of near-steady-state values after the initial rise of equatorward wave-activity flux into low latitudes. For the no-Hadley case in Fig. 9b, the two stronger forcing amplitudes (1.5 and 1.0) show a reduction in equatorward flux, indicating a return flux due to wave reflection. The time delay for reflection in the weaker forced case ($\delta = 1.0$) compared to the stronger forced case ($\delta = 1.5$) is consistent with nonlinear reflection as discussed by Magnusdottir and Haynes (1999). The Hadley case, shown in Fig. 9a, is also consistent with nonlinear reflection. Here, however, the decrease in flux is less than in the corresponding no-Hadley simulations. This is due to the damping associated with the Hadley circulation.

5. Discussion

We have shown that in the presence of a Hadley circulation, planetary waves propagating toward low latitudes in three-dimensional tropospheric flow are reflected back to midlatitudes if the forcing amplitude is large enough. Furthermore, we have shown that the Hadley circulation maintains a gradient of PV at low latitudes, resisting the PV overturning that is vital to wave reflection. The presence of a Hadley circulation therefore acts to dampen planetary wave reflection.

Our results extend earlier results in two areas. First, we generalize the results of MH99 who examined nonlinear reflection in three-dimensional tropospheric flows, but without any representation of the Hadley circulation. We also generalize the shallow water results of EPP and MW00 to fully three-dimensional flow.

Second, our results give new insight into the mechanism through which the Hadley circulation damps reflection. In a budget analysis of low-latitude pseudomomentum, EPP concluded that the direct influence of the Hadley circulation on wave reflection is small and that the influence of the thermal forcing is negligible. Instead, the Hadley circulation damps reflection through an indirect mechanism involving hyperdiffusion. In this mechanism, the Hadley circulation maintains the low-latitude PV gradient so that wave breaking continues indefinitely. The continued breaking increases the enstrophy cascade to small scales, allowing hyperdiffusion to dissipate more pseudomomentum than in the corresponding no-Hadley case. In the no-Hadley case, wave breaking quickly homogenizes the low-latitude PV, halting wave breaking and limiting the amount of pseudomomentum removed by hyperdiffusion.

Based on our results in a baroclinic model, we suggest that the Hadley circulation affects wave reflection in a more direct manner. Specifically, we believe that the thermal forcing driving the Hadley circulation inhibits PV overturning that is vital for nonlinear wave reflection. As seen in Fig. 3 for wave-3 topography and in Figs. 6 and 9 for isolated topography, when a Hadley circulation is present, there is substantially less wave breaking than in the corresponding no-Hadley case. Based on a study by Haynes and Ward (1993), who showed that the damping rate of a PV anomaly depends on its depth, it is not surprising that EPP underestimated the importance of thermal forcing. Although EPP and MW00 use thermal relaxation timescales that are shorter than that used in this study (EPP use 5 day^{-1}; MW00

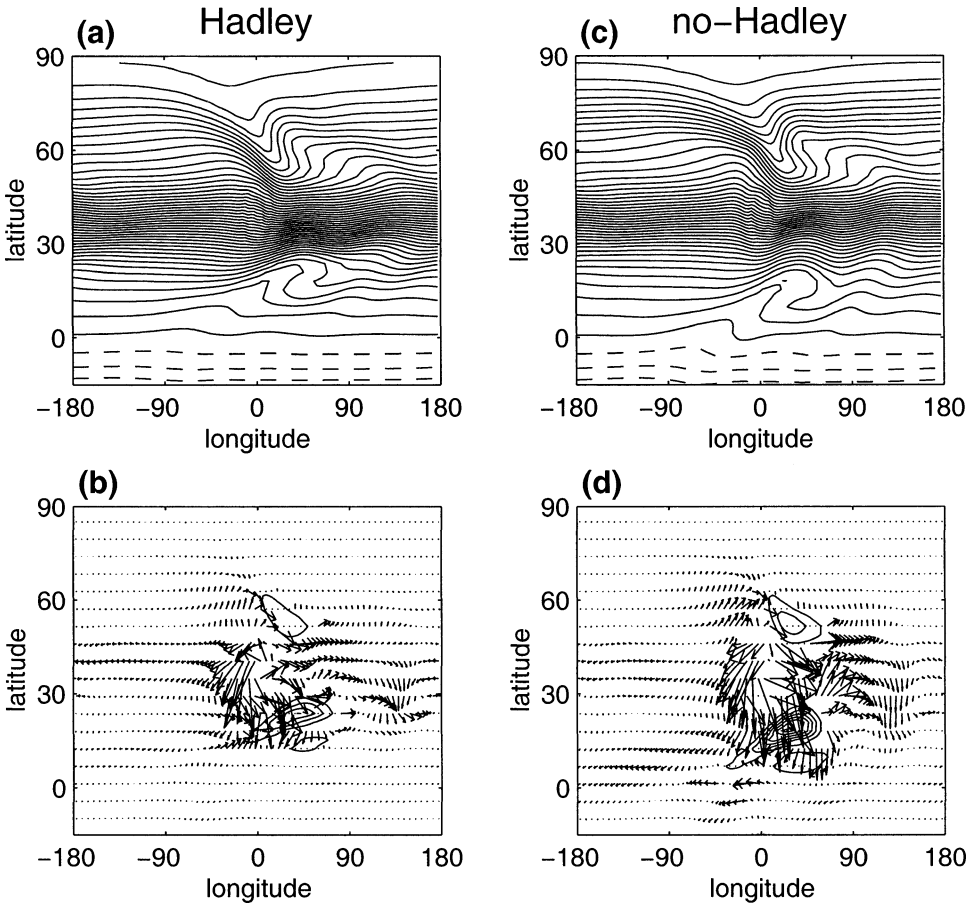

FIG. 6. Day 10 of integrations with isolated forcing of nondimensional forcing amplitude $\delta = 1.5$. PV for (a) Hadley and (c) no-Hadley initial states. Pseudomomentum flux (arrows) and pseudomomentum density (contours) for (b) Hadley and (d) no-Hadley initial state. The Hadley case is shown on the $\theta = 345$ K surface and the no-Hadley case is shown on the $\theta = 350$ K surface. Contour interval in (a) and (c) is 0.2 PVU.

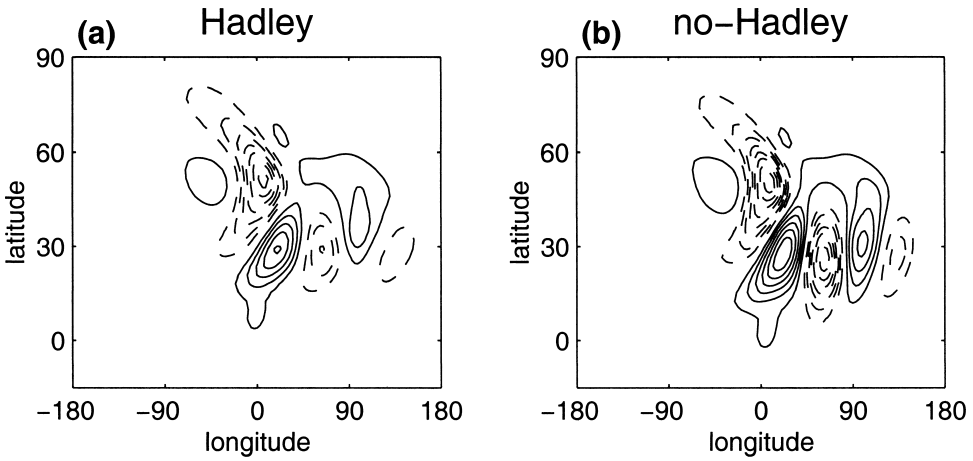

FIG. 7. Perturbation (deviation from initial state) meridional wind on the sigma = 0.2 surface on day 10 with forcing amplitude of 1.5 for (a) Hadley state and (b) no-Hadley state. Contour interval is 1.0 m s^{-1} in both cases.

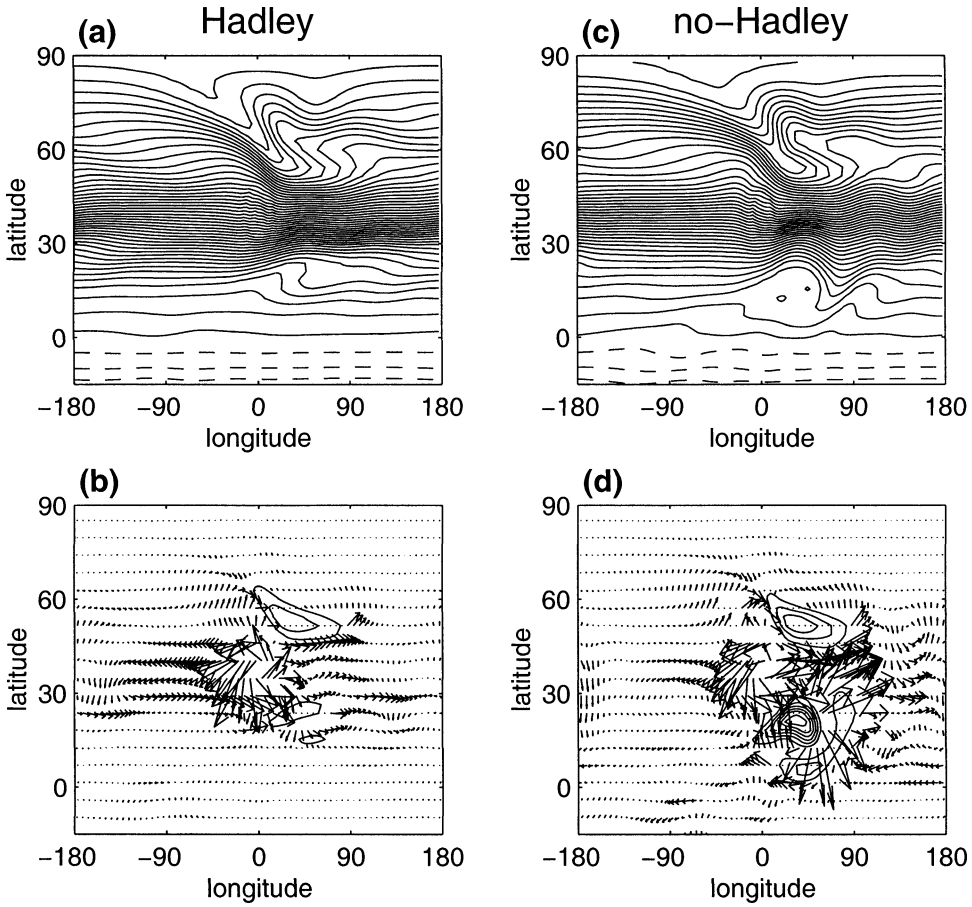

FIG. 8. Same as Fig. 6, except after 15 days.

use a value that varies in latitude, from 1 day^{-1} to 11 day^{-1}) the large relative depth of PV anomalies in the shallow water model suggests that the effective relaxation timescales are much longer.

It is worth noting that MH99 considered the effect of thermal damping on wave reflection in three-dimensional flow and found that it did affect wave reflection, but to a much lesser extent than our results indicate. They were concerned with the effect of radiative cooling, so the temperature profile to which they relaxed

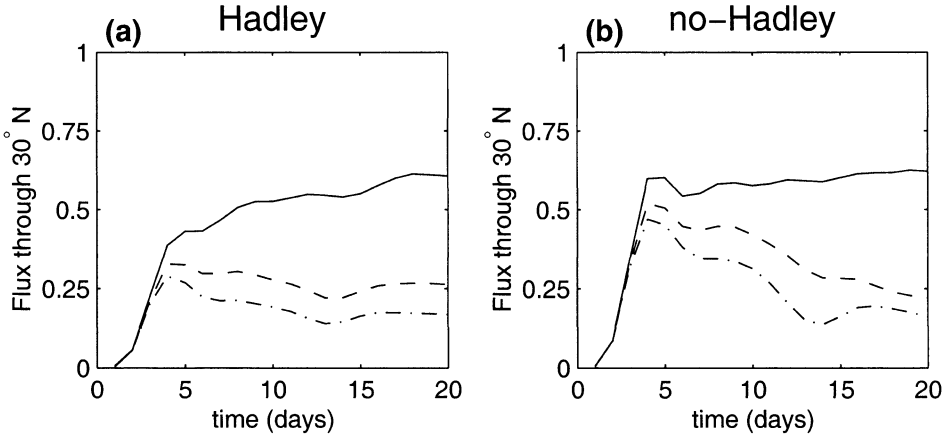

FIG. 9. Normalized (by δ squared, multiplied by 1000) meridional pseudomomentum flux through 30°N for forcing amplitudes $\delta = 0.1$ (thin solid), $\delta = 1.0$ (dashed), and $\delta = 1.5$ (dashed–dotted). Shown are profiles for the (a) Hadley state and the (b) no-Hadley state.

was the initial temperature profile (that of the basic state). Their thermal forcing was therefore substantially less intense than the thermal forcing that we use in this study, since our T_r implicitly contains a representation of low-latitude latent heating due to convection. Unlike the present study, however, MH99 applied thermal damping to all wavenumbers of the temperature field. They found that thermal damping reduced amplitudes of the various features in the response (more so for smaller relaxation timescales), but that the general pattern remained the same.

The question of whether wave reflection occurs in real tropospheric flows is still open. Dynamical and thermodynamic processes that are present in the real atmosphere and that will likely have an effect on nonlinear wave reflection are missing from our experiments. Perhaps the most obvious missing dynamical element is that of transient eddies. The transient eddy feedback, not only on the mean flow but also on stationary eddies, is thought to be significant. Here, we chose to suppress transient eddies to simplify interpretation of the large-scale waves. However, one might choose to include the transients in a study focusing on statistics of the flow rather than initial value problems such as the current study.

There have been some attempts to identify nonlinear reflection in general circulation model (GCM) experiments. Schneider (1990) analyzed GCM simulations by using a linear stationary wave model based on the GCM. Using comparisons of the full GCM results with results from the linearized model, he concluded that nonlinear reflection from a low-latitude critical line was possible. Cook and Held (1992) used a low-resolution (R15) aquaplanet GCM, forced with annual mean solar radiation, to investigate the role of nonlinearities on orographically forced planetary waves. They did not find any evidence of reflection, but suggested that the coarse resolution of the model may have interfered with nonlinear reflection. It would be of great interest to repeat the type of experiments that Cook and Held (1992) carried out, but in a higher-resolution GCM. [MH99 examined the sensitivity of nonlinear reflection on spatial resolution and found that a minimum resolution greater than that used by Cook and Held (1992) is required.] This is the topic of a forthcoming paper.

Observational studies have noted some evidence of reflection. Perhaps the clearest such study is that of Schubert and Park (1991) using European Centre for Medium-Range Weather Forecasts (ECMWF) winter data from 1981–87. Their Fig. 9b indicates strong wave activity flux from low to high latitudes in the central Pacific region. This is apparently due to significant reflection in the vicinity of the equatorward flank of the east Asian jet.

6. Conclusions

We have investigated planetary wave reflection in the presence of a Hadley circulation in a primitive equation model. Our key conclusions are as follows.

- The Hadley circulation damps nonlinear planetary wave reflection, but given enough forcing, reflection will still occur.
- Thermal forcing used to drive the Hadley circulation has a much greater influence in the primitive equation case than in the shallow water case.
- The Hadley circulation inhibits wave reflection through thermal forcing, which resists the PV overturning critical to wave reflection.

Acknowledgments. We thank Dr. Mike Blackburn for his advice on the primitive equation model used in this study and three anonymous reviewers for helpful comments on the manuscript. This work was supported by NSF Grant ATM-9908883 and by NASA Grant NGT5-03203.

APPENDIX A

Effect of Vertical Momentum Diffusion

The value of diffusivity that we use in the vertical momentum diffusion is substantially larger than the values used by Held and Hou (1980), which ranged from 0.5 to 25 $m^2\ s^{-1}$. Although vertical momentum diffusion is only applied to the zonally symmetric component of the flow, it is possible that it changes the character of wave propagation and breaking, preventing a direct comparison between the Hadley initial state (which has the diffusion) and the no-Hadley initial state (which does not have the diffusion).

To evaluate the effect of vertical diffusion, it was applied to the no-Hadley initial state with values of vertical diffusivity as high as 100 $m^2\ s^{-1}$. In each case, planetary waves were forced with isolated topography with a nondimensional forcing amplitude of 1.0. In the Hadley case, the influence of diffusion on the background flow is exactly balanced by the thermal forcing. In this case, however, there is no thermal forcing, so without additional forcing, the diffusion will change the background flow in time. To prevent this drift, we add an additional forcing on the zonal component of the flow to balance the effect of diffusion.

Figure A1 shows PV after 12 days on the $\theta = 350$ K surface for a case without diffusion and for a case with $\nu = 75\ m^2\ s^{-1}$, respectively. Wave breaking is clearly occurring for both cases in Fig. A1, visible around 15°N, 30°W. There are only slight differences between the PV fields for the different diffusivities, indicating that vertical momentum diffusion does not play a major role in the results on wave reflection reported in sections 3 and 4.

APPENDIX B

Wave Activity Diagnostics

We apply the pseudomomentum diagnostics derived for the primitive equations by Haynes (1988). For brev-

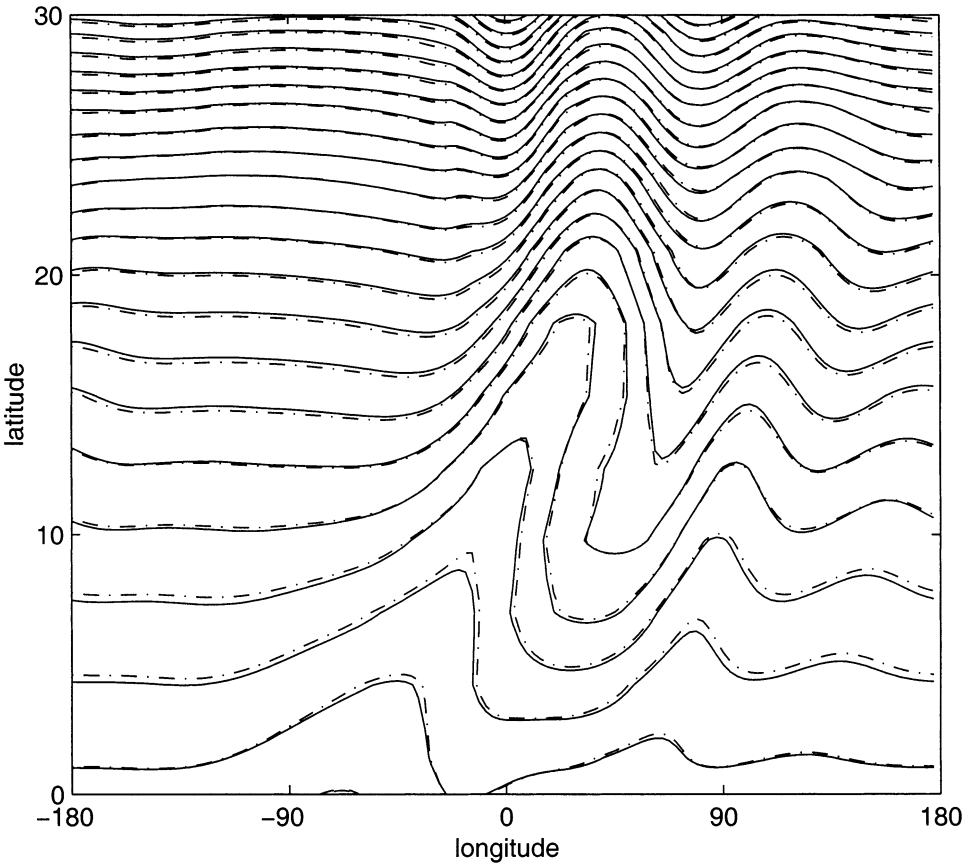

FIG. A1. Potential vorticity on the $\theta = 350$ K surface after 12 days for two simulations. The solid contours correspond to a simulation with no vertical diffusion. The dashed–dotted contours are for a simulation with a diffusion coefficient of 75 $m^2\ s^{-1}$. The flow is forced with an isolated Gaussian mountain [nondimensional amplitude (δ) of 1.0] located at 40°N, 0°.

ity, only a short description is given here. A more detailed description of their application to the primitive equations can be found in MH99 and Magnusdottir and Haynes (1996). The flow fields are decomposed into zonally symmetric basic-state parts, denoted by $(\ \cdot\ )_0$ and deviations from the basic-state part, denoted by $(\ \cdot\ )_e$. The conservation relation for angular pseudomomentum, which is expressed in isentropic coordinates, is given by

$$\frac{\partial A}{\partial t} + \nabla \cdot \mathbf{F} = \frac{\partial A}{\partial t} + \frac{1}{a\cos\phi}\frac{\partial F^{(\lambda)}}{\partial \lambda} + \frac{1}{a\cos\phi}\frac{\partial (F^{(\phi)}\cos\phi)}{\partial \phi} + \frac{\partial F^{(\theta)}}{\partial \theta} = S, \tag{B.1}$$

where S only contains nonconservative terms, A is the pseudomomentum density, given by

$$A = -\sigma_e u_e \cos\phi + \sigma \int_0^{P_e} [m_0(P_0 + \tilde{P}) - m_0(P_0)]\, d\tilde{P}, \tag{B.2}$$

and the components of the flux $\mathbf{F}$ are given by

$$F^{(\lambda)} = uA - \frac{1}{2}\sigma_0(u_e^2 - v_e^2)\cos\phi - \tau(p_e, p_0, \theta)\cos\phi + \frac{\partial}{a\partial\phi}\Psi_1 + \frac{\partial}{\partial\theta}\Psi_2, \tag{B.3a}$$

$$F^{(\phi)} = vA - \sigma_0 v_e u_e \cos\phi - \frac{\partial}{a\cos\phi\partial\lambda}\Psi_1, \tag{B.3b}$$

$$F^{(\theta)} = g^{-1}a^{-1}p_e M_{e\lambda} - \frac{\partial}{a\cos\phi\partial\lambda}\Psi_2. \tag{B.3c}$$

Other variables are defined as follows: p is pressure, $\sigma = -g^{-1}\partial p/\partial\theta$ is mass density in isentropic coordinates, $P = \sigma^{-1}[2\Omega\sin\phi + (\partial v/a\cos\phi\partial\lambda) - (\partial u\cos\phi/a\cos\phi\partial\phi)]$ is potential vorticity, and $M = \Pi\theta + gz$ is the Montgomery streamfunction, with $\Pi = c_p(p/p_s)^{\kappa}$, where $p_s = 1000$ hPa. The basic-state variable m_0 is given by

$$m_0[P_0(\phi, \theta)] = \int_0^{\phi} \sigma_0(\tilde{\phi})\cos\tilde{\phi}\, d\tilde{\phi}, \tag{B.4}$$

and can be thought of as a measure of a particle's lat-

itudinal position relative to its position in the basic state. The function τ is defined as

$$\tau(p_e, p_0, \theta) = g^{-1} \int_0^{p_e} \frac{\kappa\tilde{p}}{(p_0 + \tilde{p})} \Pi(p_0 + \tilde{p}, \theta)\, d\tilde{p}. \tag{B.5}$$

The terms involving Ψ_1 and Ψ_2 in the definition of the flux are correction terms, derived in MH99, so that the flux is not phase dependent. Note that the addition of these terms does not change the conservation relation in (B.2) since their divergence is zero.

The source term S, which only contains nonconservative contributions, is given in Haynes (1988). Here we rewrite this term to show contributions from the different forcing mechanisms used to drive the Hadley circulation. (The topographic source term is not included since we only apply this relation away from the wave source.) The dissipation due to thermal and momentum forcing is further divided into dissipation acting on the basic state (Hadley cell dissipation) and dissipation acting on the eddies (eddy heating dissipation and eddy friction dissipation), so that the following terms are considered:

$$\begin{aligned}
S = {} & \cos\phi(\sigma\dot{\theta})_{0\theta}(X - m_e P) - m_e \cos\phi a^{-1}[F_0 - \dot{\theta}_0 u_{0\theta}]_\phi + \sigma_e \cos^2\phi(\sigma_e v_0 \zeta_0 - \sigma_0 v_0 \zeta_e)\Big] && \text{Hadley cell dissipation} \\
& + \cos\phi(\sigma\dot{\theta})_{e\theta}(X - m_e P - u_e \cos\phi) + \sigma(\dot{\theta}u_\theta)_e \cos^2\phi \Big] && \\
& + a^{-1} m_e \left[\frac{\partial}{\partial\phi}(\cos\phi\dot{\theta}u_\theta)_e - \frac{\partial}{\partial\lambda}(\dot{\theta}v_\theta)_e\right] \Bigg\} && \text{eddy heating dissipation} \\
& + a^{-1} m_e \left[\frac{\partial}{\partial\lambda}(G)_e - \frac{\partial}{\partial\phi}(F\cos\phi)_e\right] - F_e \sigma_e \cos^2\phi \Bigg\} && \text{eddy friction dissipation} \\
& + \cos\phi(\sigma\dot{\theta}_D)_{e\theta}(X - m_e P - u_e \cos\phi) + \sigma(\dot{\theta}_D u_\theta)_e \cos^2\phi \Big] && \\
& + a^{-1} m_e \left[\frac{\partial}{\partial\phi}(\cos\phi\dot{\theta}_D u_\theta)_e - \frac{\partial}{\partial\lambda}(\dot{\theta}_D v_\theta)_e\right] \Bigg\} && \text{hyperdiffusion dissipation,} \\
& + a^{-1} m_e \left[\frac{\partial}{\partial\lambda}(G_D)_e - \frac{\partial}{\partial\phi}(F_D\cos\phi)_e\right] - (F_D)_e \sigma_e \cos^2\phi \Big] &&
\end{aligned} \tag{B.6}$$

where $\dot{\theta}$ is the diabatic heating associated with thermal relaxation, ζ is absolute vorticity, terms with a subscript D correspond to forcing from hyperdiffusion, F and G represent the influence of vertical diffusion on the u and v components of the wind, respectively, and

$$X = \int_0^{P_e} [m(P_0 + \tilde{P}) - m(P_0)]\, d\tilde{P}. \tag{B.7}$$

Note that σX is the dominant term in the definition of pseudomomentum density (A) in (B.2). It is the pseudomomentum density due to the balanced part of the flow, or due to the rearrangement of PV.

REFERENCES

Brunet, G., and P. H. Haynes, 1996: Low-latitude reflection of Rossby wave trains. *J. Atmos. Sci.,* **53,** 482–496.

Cook, K. H., and I. H. Held, 1992: The stationary response to large-scale orography in a general circulation model and a linear model. *J. Atmos. Sci.,* **49,** 525–539.

Esler, J. G., L. M. Polvani, and R. A. Plumb, 2000: The effect of the Hadley circulation on the propagation and reflection of planetary waves in a simple one-layer model. *J. Atmos. Sci.,* **57,** 1536–1556.

Grose, W. L., and B. J. Hoskins, 1979: On the influence of orography on the large-scale atmospheric flow. *J. Atmos. Sci.,* **36,** 223–234.

Haynes, P. H., 1988: Forced, dissipative generalizations of finite-amplitude wave-activity conservation relations for zonal and nonzonal basic flows. *J. Atmos. Sci.,* **45,** 2352–2362.

——, and W. E. Ward, 1993: The effect of realistic radiative transfer on potential vorticity structures, including the influence of background shear and strain. *J. Atmos. Sci.,* **50,** 3431–3453.

Held, I. M., 1985: Pseudomomentum and the orthogonality of modes in shear flows. *J. Atmos. Sci.,* **42,** 2280–2288.

——, and A. Y. Hou, 1980: Nonlinear axially symmetric circulations in a nearly inviscid atmosphere. *J. Atmos. Sci.,* **37,** 515–533.

——, and P. J. Phillips, 1990: A barotropic model of the interaction between the Hadley cell and a Rossby wave. *J. Atmos. Sci.,* **47,** 856–869.

Hoskins, B. J., and A. J. Simmons, 1975: A multi-layer spectral model and the semi-implicit method. *Quart. J. Roy. Meteor. Soc.,* **101,** 637–655.

Hsu, H.-H., B. J. Hoskins, and F.-F. Jin, 1990: The 1985/86 intraseasonal oscillation and the role of the extratropics. *J. Atmos. Sci.,* **47,** 823–839.

Kiehl, J. T., J. J. Hack, G. B. Bonan, B. A. Boville, B. P. Briegleb,

D. L. Williamson, and P. J. Rasch, 1996: Description of the NCAR Community Climate Model (CCM3). NCAR Tech. Rep. TN-420+STR, 152 pp.

Killworth, P. D., and M. E. McIntyre, 1985: Do Rossby-wave critical layers absorb, reflect, or over-reflect? *J. Fluid Mech.,* **161,** 449–492.

Magnusdottir, G., and P. H. Haynes, 1996: Wave activity diagnostics applied to baroclinic wave life cycles. *J. Atmos. Sci.,* **53,** 2317–2353.

——, and ——, 1999: Reflection of planetary waves in three-dimensional tropospheric flows. *J. Atmos. Sci.,* **56,** 652–670.

——, and C. Walker, 2000: On the effects of the Hadley circulation and westerly equatorial flow on planetary-wave reflection. *Quart. J. Roy. Meteor. Soc.,* **126,** 2725–2745.

Postel, G. A., and M. H. Hitchman, 1999: A climatology of Rossby wave breaking along the subtropical tropopause. *J. Atmos. Sci.,* **56,** 359–373.

Schneider, E. K., 1990: Linear diagnosis of stationary waves in a general circulation model. *J. Atmos. Sci.,* **47,** 2925–2952.

Schubert, S. D., and C.-K. Park, 1991: Low-frequency intraseasonal tropical–extratropical interactions. *J. Atmos. Sci.,* **48,** 629–650.

Watterson, I. G., and E. K. Schneider, 1987: The effect of the Hadley circulation on the meridional propagation of stationary waves. *Quart. J. Roy. Meteor. Soc.,* **113,** 779–813.

Waugh, D. W., L. M. Polvani, and R. A. Plumb, 1994: Nonlinear, barotropic response to a localized topographic forcing: Formation of a ''tropical surf zone'' and its effect on interhemispheric propagation. *J. Atmos. Sci.,* **51,** 1401–1416.